JOURNAL OF CATALYSIS 27, 311-321 (1972)

Studies on Catalysis by Molten Metal. V. Kinetics of the Dehydrogenation of sec-Butyl Alcohol over the Liquid Indium Catalyst

AKIRA MIYAMOTO AND YOSHISADA OGINO

Department of Chemical Engineering, Faculty of Engineering, Tohoku University, Aramaki Aoba, Sendai, Japan

Received May 9, 1972

The dehydrogenation of *sec*-butyl alcohol was studied by using a device of rectangular duct type reactor containing liquid indium catalyst. The experimental conditions were as follows: temperature 450–550°C, total pressure 1 atm, partial pressure of alcohol 0.1–0.4 atm, feed rate of alcohol 0.0937–0.6 mole/hr.

The experimental results were found to obey a Langmuir-type rate equation, $W = k_1^0\rho_A/(1 + K_AP_A)$, which indicates that the surface unimolecular decomposition will be the rate controlling step. The respective values of K_A and k_1^0 were 1×10^{-3} exp $(13{,}000/RT)$ atm^{-1} and 3×10^6 exp $(-28{,}000/RT)$ cm/sec.

The comparison of the experimental value of K_A with the value estimated by statistical thermodynamics suggested that the adsorbed alcohol may be mobile on the surface of liquid indium. Further, the assumption of a mobile activated complex gave a theoretical k_1^0 value which agrees fairly well with the experimentally determined value of k_1^0.

INTRODUCTION

In the previous works (*1–4*) of this series which treated the catalyses of liquid metals, the authors found that some liquid metals such as zinc, indium, gallium, thallium, and aluminum catalyze the dehydrogenations of alcohols and amines with considerably high selectivities. It was also revealed that the activities of liquid metals persist for a long period. In view of a primary importance to obtain a general survey on the catalyses of the liquid metals, attention of the authors in the previous works were given to the qualitative aspects of the activities of the liquid metal catalysts. Therefore, theoretical considerations to the experimental results were not given in the previous papers, though the papers demonstrated that the liquid metals have undoubtedly their own catalytic activities.

Now, more precise experimental data which afford theoretical treatments seem to be required to obtain further information about the catalyses of the liquid metals. Considering this situation, the present authors have undertaken a kinetic study to clarify the mechanism of the dehydrogenation of *sec*-butyl alcohol over the liquid indium catalyst. The purpose of this paper is to describe not only the experimental results but also the details of the theoretical analyses of the experimental data.

EXPERIMENTAL

Catalyst. Indium of 99.999% purity was used as a catalyst. The reasons for the use of this metal are as follows: (i) Among the catalytically active metals in their liquid states, indium is a metal which is obtainable most easily and it has a satisfactorily high purity. (ii) Oxide of indium which will be present inevitably in and over the raw metal can be reduced easily to indium metal by exposing the raw metal to the reaction atmosphere (or by streaming purified hydrogen over the metal which

is kept at high temperatures). Thus, the measurement of the catalytic activity of the pure metal was thought to be possible.

Reactant. A. G. R. grade of *sec*-butyl alcohol (*sec*-BuOH) was used as a reactant. According to the previous work (*2*), this alcohol can be dehydrogenated with high conversions and high selectivities. Therefore, it was thought that the use of this alcohol as a reactant is adequate to measure precise kinetic data with little interference from side reactions.

Apparatus and procedures. A schematic diagram of the experimental apparatus is given in Fig. 1. As can be seen in this figure, the reaction system belongs to a flow type. The reactant alcohol was fed by a calibrated microfeeder ① into a preheater ②, where the reactant was vaporized and mixed with purified helium. Then, the vapor was led to a rectangular duct-type reactor ③ containing liquid indium catalyst ④. By handling a preheated syringe (2 m*l*), a small amount of sample containing reaction products was taken through a rubber cap mounted on a small port ⑤. The sample was analyzed by gas chromatography (analysis I). The main stream of the effluents from the reactor was cooled by a condenser ⑥. The condensates collected in both separators ⑦ and ⑧ as well as the gas sample taken from a port ⑨ were analyzed by the gas chromatography (analysis II). The result of the analysis I was compared with that of the analysis II to check the sampling error.*

The rectangular duct-type reactor employed in this work was made from pyrex glass. The details of the geometry of the reactor are given in Fig. 2. The electric furnace which served to heat the reactor was made from two concentric pyrex tubes. The inner tube served to support the nichrome heater and the outer tube served as an insulator. By the use of this furnace, a visual observation of the catalyst in the reactor became possible.

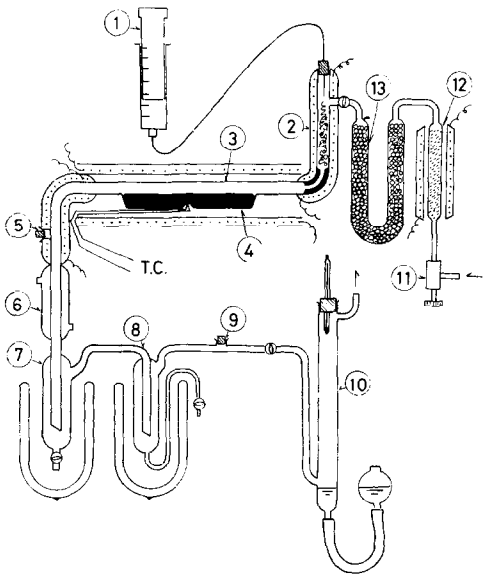

FIG. 1. The schematic diagram of the experimental apparatus; ① microfeeder, ② preheater, ③ reactor, ④ catalyst (liquid indium), ⑤ sampling port for vapor mixture, ⑥ condenser, ⑦ separator, ⑧ separator, ⑨ sampling port for gaseous mixture, ⑩ film flowmeter, ⑪ valve for helium reservoir, ⑫ deoxo catalyst, and ⑬ molecular sieve drierite.

RESULTS

Life of catalyst. The observed catalytic activity declined little throughout the whole duration (about 1 year) of the present work. Therefore, it can be said that little catalyst fouling occurred during the present work.

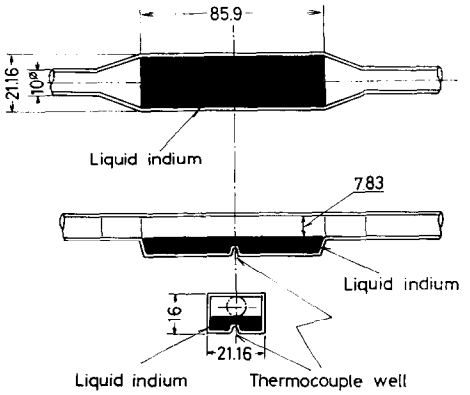

FIG. 2. Details of the rectangular duct-type reactor (dimensions are expressed in mm).

* When the reactant was diluted with helium, the analysis II gave inaccurate results but the results of the analysis I were reliable. On the other hand, when the reactant was not diluted, the results of both analysis I and analysis II were identical.

Selectivity. Results of gas chromatographic analyses showed that little side reactions occurred in the temperature range of 400–500°C. Namely, methane contents in the gaseous products were less than 5% and the respective contents of carbon monoxide and carbon dioxide were less than 0.1%, and the main component in the gaseous products was found to be hydrogen. Further, the liquid products were found to contain more than 95% of methyl ethyl ketone (MEK).

Degree of conversion. The relation between the conversion of *sec*-BuOH and the reaction temperature is given in Fig. 3, wherein the relation obtained under a constant feed rate of *sec*-BuOH (0.0937 mole/hr) is illustrated, and the effects of varying feed rate on the conversion are seen in Fig. 4. An example of relation between the conversion and the mean partial pressure of alcohol ($\bar{P}_A$) is given in Fig. 5 (the mean partial pressure was defined by an arithmetic mean of the partial pressure of alcohol in the feed vapor and that in the exit vapor). This figure expresses implicitly the effect of dilution of alcohol vapor with helium.

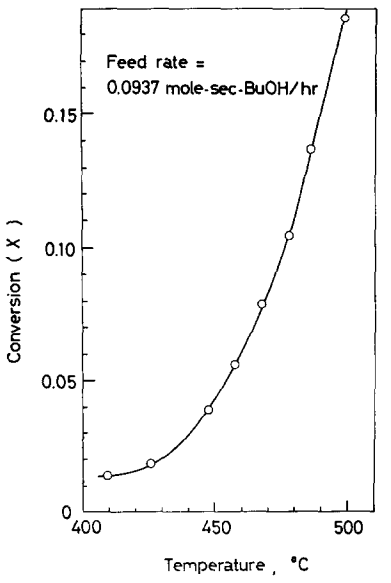

FIG. 3. The relation between the degree of conversion of *sec*-BuOH to methyl ethyl ketone (MEK) and the reaction temperature at a feed rate of 0.0937 mole/hr (the alcohol vapor was not diluted with helium).

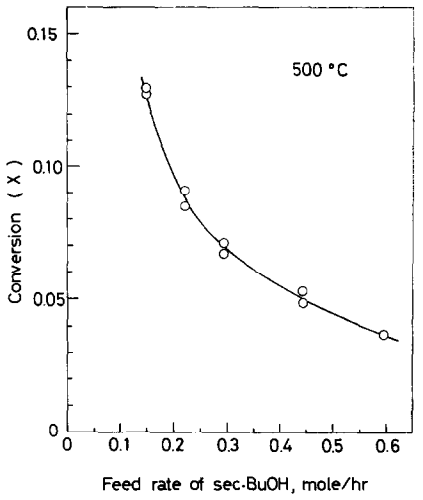

FIG. 4. The effect of feed rate of *sec*-BuOH (undiluted with helium) on the degree of conversion at 500°C.

DISCUSSION

Mathematical Analysis of the Rectangular Duct-Type Reactor.

A method of mathematical analysis of the rectangular duct type reactor had been given by Solbrig and Gidaspow (*5*; see appendix). Their method was found to be applicable satisfactorily to the reactor analyses in the present work (see Appendix). Extensions and simplifications of their treatment were examined and the results will be given below.

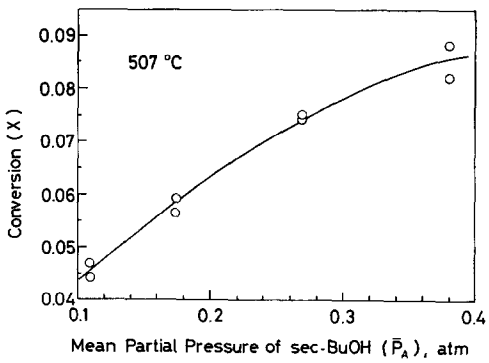

FIG. 5. The effect of the mean partial pressure ($\bar{P}_A$) of *sec*-BuOH on the degree of conversion at 507°C.

The application of the method of Solbrig and Gidaspow to the present reactor with $n = 1$ (first order reaction) gave results as shown in Fig. 6 (numerical computations were carried out with an NEAC 2200 – Model 700 digital computer: Computer Center, Tohoku University). This figure indicates that the reaction constant k_1 can be evaluated by assigning the mixing cup dimensionless concentration C_b at a given dimensionless distance x from the inlet. Since the dimensionless distance x is given by $x = \eta/1.5 \times (Ua^2/D_{Ae})$ and the degree of conversion X is defined by $X = 1 - C_b$, the relations given in the figure may be abbreviated as follows,

$$k_1 = F_0(D_{Ae}, U, X), \qquad (1)$$

where F_0 is a function of D_{Ae}, U and X.

It must be pointed out that the reaction constant k_1 is independent of the diffusion coefficient under the present experimental conditions and with the dimensions of the present reactor. Namely, as illustrated in Fig. 7, the degree of conversion X was found to be fairly constant irrespective of the values of D_{Ae} if values of U and k_1 were fixed. Therefore, the following expression may be a good approximation of Eq. (1):

$$k_1 = F_1(U, X), \qquad (2)$$

where F_1 is a function to be determined

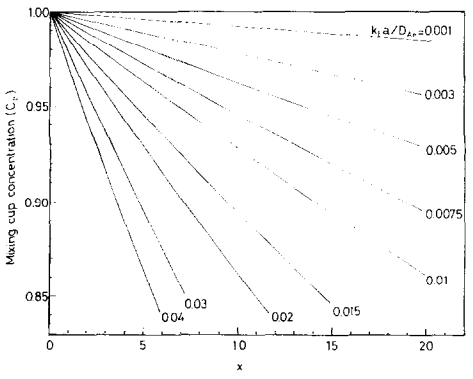

FIG. 6. Theoretical curves expressing the relation between the dimensionless mixing-cup concentration (C_b) for the apparent first order reaction ($n = 1$) and the dimensionless distance (x) from the inlet of the reactor.

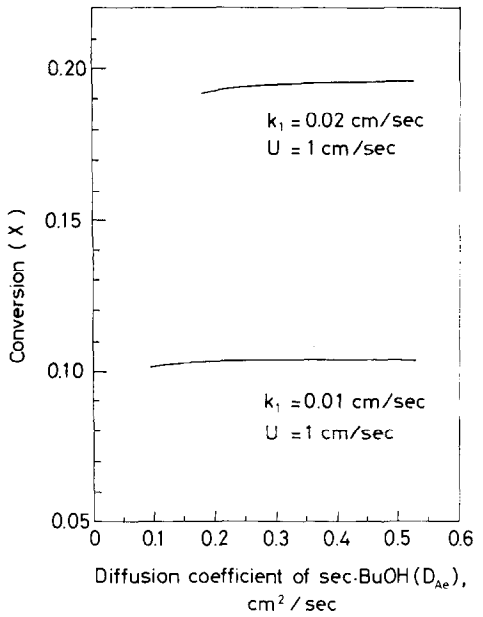

FIG. 7. Effects of diffusion coefficient (D_{Ae}) of *sec*-BuOH vapor on the estimated degree of conversion.

explicitly. The straight line relationship given in Fig. 8, wherein values of k_1/U are plotted against $\log_{10}\{1/(1 - X)\}$, indicates that the explicit form of Eq. (2) is

$$k_1 = 0.2115 \cdot U \cdot \log_{10}\{1/(1 - X)\}. \qquad (3)$$

The simple form of this equation will

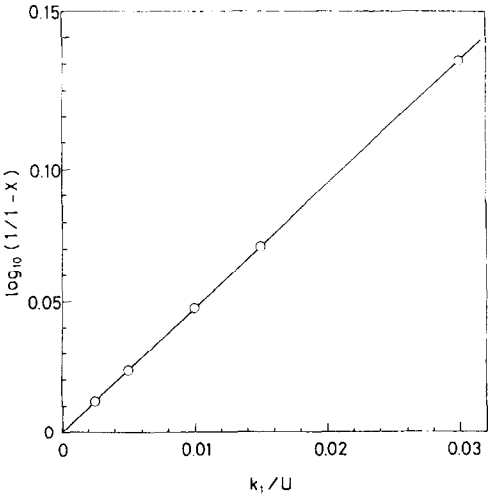

FIG. 8. The universal linear "$\log_{10}(1/1 - X)$–k_1/U" relationship exemplified by the calculated points for k_1 = 0.01 cm/sec and k_1 = 0.03 cm/sec.

greatly simplify the treatment of the experimental data, and it should be compared with the complicated original treatment (see Appendix).

The possibility of a further extension of the present treatment seems to be suggested by comparing Eq. (3) with the following simple kinetic treatment. Namely, if a simple first order reaction with respect to the reactant is assumed, the reaction rate V will be given by

$$V = \rho_{Ao} \cdot dX/d(A/SU) = k_1 \cdot \rho_{Ao}(1 - X) = k_1 \cdot \rho_A, \quad (4)$$

where A is the geometrical surface area of the catalyst and S is the cross-sectional area of the duct. The integration of Eq. (4) yields

$$k_1 = (SU/A) \cdot \ln\{1/(1 - X)\}. \quad (5)$$

The geometry of the reactor gives $S/A = 0.0911$. Therefore, Eq. (5) can be converted to

$$k_1 = 0.2092 \cdot U \cdot \log_{10}\{1/(1 - X)\}. \quad (6)$$

The right-hand side of this equation is almost equivalent to that of Eq. (3). This result indicates that the kinetics for the first-order reaction in the reactor with the geometry and the experimental conditions employed in the present work can be treated by assuming simply Eq. (4) without any complicated treatments as used by Solbrig and Gidaspow. This result prompted the authors to examine a more realistic rate equation as a boundary condition of the rectangular duct-type reactor.

Extensions and Approximations of the Mathematical Analysis

A more realistic rate equation for the surface catalysis is a Langmuir-type equation. Thus, the following Langmuir-type rate equation was considered in this work:

$$V = k_1^0 \cdot \rho_A/(1 + K_A \cdot P_A), \quad (7)$$

where k_1^0 is a rate constant, K_A is an adsorption coefficient for the reactant, and P_A is a partial pressure of the reactant. The discussions in the preceding section will give the expectation that the solution of the following differential equation may be a good approximation of the exact solution based on the treatment of Solbrig and Gidaspow:

$$V = \rho_{Ao} \cdot dX/d(A/SU) = \rho_{Ao} \cdot k_1^0 \cdot (1 - X)/\{1 + K_A \cdot P_A^0(1 - X)\}. \quad (8)$$

Putting the relation

$$x = (2/3) \cdot (D_{Ae}/Ua) \cdot (\eta/a) = 37.3 \cdot (D_{Ae}/U)$$

into the integrated formula of Eq. (8) yields the following equation,

$$\ln\{1/(1 - X)\} + K_A \cdot P_A^0 \cdot X = 0.75 \cdot x \cdot (k_1^0 \cdot a/D_{Ae}). \quad (9)$$

On the other hand, the exact numerical solution of the partial differential equation given by Solbrig and Gidaspow with the boundary condition

$$\begin{cases} \partial C/\partial y(x, -1, z) = K_{w1} \cdot C \\ K_{w1} = k_1^0 \cdot a/D_{Ae} \cdot (1 + K_A \cdot P_A), \end{cases} \quad (10)$$

in place of an original boundary condition (6a) (see Appendix) gave results as exemplified in Fig. 9. This figure gives the following relation.

$$\ln\{1/(1 - X)\} + K_A \cdot P_A^0 \cdot X = 0.0075 \cdot x. \quad (11)$$

Since the figure shows an $X - x$ relation for the case of $k_1^0 a/D_{Ae} = 0.01$, the following relation

$$\ln\{1/(1 - X)\} + K_A \cdot P_A^0 \cdot X = 0.75 \cdot x \cdot (k_1^0 \cdot a/D_{Ae}),$$

results from Eq. (11). Thus, the validity of the use of Eq. (9) for the analysis of the experimental result was established.

A modification of Eq. (9) gives a convenient formula for the application of the theory to the experimental data. When the conversion has a small value, the following approximations may be permitted,

$$\ln\{1/(1 - X)\} \simeq X + X^2/2 \quad (12)$$

and

$$X \simeq X - X^3/4 = (X + X^2/2) \cdot (1 - (X)/2). \quad (13)$$

These two equations give

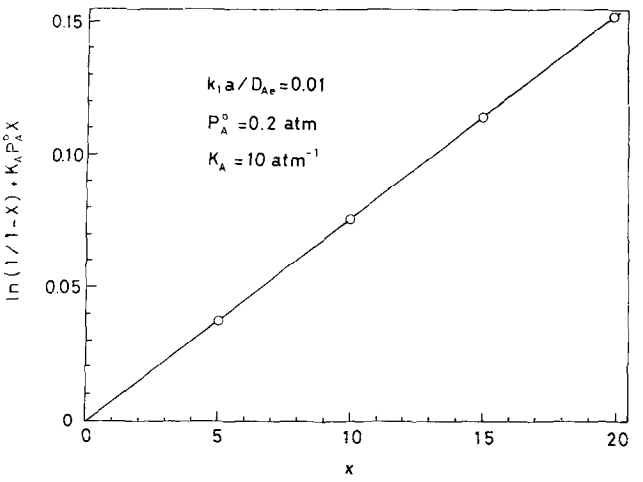

FIG. 9. The linear "$\ln(1/1 - X) + K_A P_A^0 X$—$x$" relationship exemplified by the calculated point (○) for $k_l a/D_{Ae} = 0.01$, $P_A^0 = 0.2$ atm and $K_A = 10$ atm^{-1}.

$$X \simeq [\ln\{1/(1 - X)\}] \cdot (1 - X/2). \quad (14)$$

This equation with Eq. (9) yields

$$[\ln\{1/(1 - X)\}] \cdot \{1 + K_A \cdot P_A^0 \cdot (1 - X/2)\} = k_l^0 \cdot (A/SU) \quad (15)$$

The mean partial pressure $\bar{P}_A$ of the reactant is defined by

$$\bar{P}_A = 0.5 \cdot \{P_A^0 + P_A^0 \cdot (1 - X)\} = P_A^0 \cdot (1 - X/2). \quad (16)$$

Therefore, Eq. (15) can be rewritten as

$$(1/k_l^0) \cdot (1 + K_A \cdot \bar{P}_A) = (A/SU)/\ln\{1/(1 - X)\}. \quad (17)$$

The right-hand side of this equation can be evaluated from the experimental data and experimental conditions. Thus, when a reaction obeys the assumed Langmuir-type kinetics, plots of $(A/SU)/\ln\{1/(1 - X)\}$ against $\bar{P}_A$ should give a straight line. The reaction rate constant k_l^0 and the adsorption coefficient K_A can be evaluated from the intercept with the ordinate and the slope of the straight line.

Kinetic Parameters for the Dehydrogenation of sec-BuOH.

The kinetic relation given by Eq. (17) was able to apply satisfactorily to the analyses of the experimental data for the dehydrogenation of *sec*-BuOH, and values of kinetic parameters (k_l^0 and K_A) were obtainable. Plots of $\bar{P}_A$ against $(A/SU)/\{\ln(1/1 - X)\}$ gave straight lines, as shown in Fig. 10. This means that the kinetics of the dehydrogenation of *sec*-BuOH obeys the Langmuir-type rate equation, i.e., Eq. (7).

The values of k_l^0 and K_A were evaluated from the slope and the intercept with the ordinate of the straight line shown in Fig. 10. The temperature dependences of k_l^0

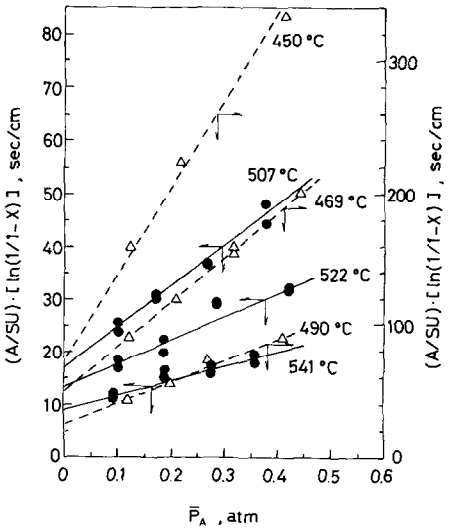

FIG. 10. Linear relationships between $(A/SU)\{\ln(1/1 - X)\}$ and $\bar{P}_A$ at various reaction temperatures.

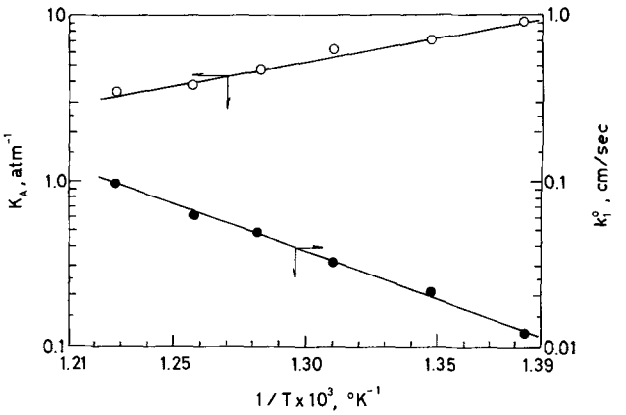

FIG. 11. The temperature dependences of the rate constant k_1^0 (●) and the adsorption coefficient K_A (○).

and K_A are shown in Fig. 11. Both log k_1^0 and log K_A showed good straight-line relationships with the reciprocal of absolute temperature $1/T$, and the following expressions for k_1^0 and K_A were obtained,

$$k_1^0 = 3 \times 10^6 \exp(-28{,}000/RT); \text{ molecules/(cm}^2\text{sec)(molecules/cm}^3\text{)}; \quad (18)$$

$$K_A = 1 \times 10^{-3} \exp(13{,}000/RT); \text{ atm}^{-1}. \quad (19)$$

Adsorbed State, Possible Reaction Schemes

The successful application of Eq. (7) [or Eq. (17)] to the experimental data indicates that a unimolecular surface dehydrogenation of the adsorbed *sec*-BuOH is the rate-controlling step of the overall reaction. Further, the adsorption of hydrogen as well as adsorption of MEK on the liquid metal seem to be weak because the denominator in Eq. (7) does not include adsorption terms for hydrogen and MEK, i.e., $K_{H_2}P_{H_2}$ and $K_{MEK}P_{MEK}$. Therefore, the following reaction scheme is probable:

sec-BuOH (g) + S $\rightleftharpoons$ *sec*-BuOH*; (Adsorption)

sec-BuOH* $\rightarrow$ H_2 (g) + MEK (g) + S, (Unimolecular surface dehydrogenation)

where * denotes an adsorbed state and S denotes an elementary section on which the adsorption is taking place (tentatively the section is called "active center" in the present paper).

It is interesting to discuss whether the adsorbed molecule of *sec*-BuOH is immobile or mobile. Statistical thermodynamics is a useful tool for this purpose. If we define the immobile adsorption as an adsorption in which the adsorbate molecule is bound by a translating surface atom of the liquid metal, the adsorption coefficient K_A is given by

$$K_A = (1/\boldsymbol{k}T) \cdot \{h/(2\pi m\boldsymbol{k}T)^{1/2}\}^3 \times (F_a/b_g \cdot F_s) \cdot \exp(q/\boldsymbol{k}T), \quad (20)$$

where $F_a = f_a^{tr} \cdot b_a$, $F_s = f_s^{tr}$, and f_a^{tr}, f_s^{tr}, b_g, and b_a are a translational partition function of adsorbed alcohol, a translational partition function of active center, an internal partition function of gaseous alcohol, and an internal partition function of adsorbed alcohol, respectively. The other quantities were expressed with the usual notations.

The approximation $f_a^{tr} \simeq f_s^{tr}$ seems to be adequate because the adsorbed molecule has been assumed to be bound by the translating (two-dimensional) active center. Further, the rotational freedom of the adsorbed molecule will be smaller than that of the gaseous molecule. Therefore, $b_a < b_g$. On combining these approximations with Eq. (20), the following inequality results:

$$K_A < (1/\boldsymbol{k}T) \cdot \{h/(2\pi m\boldsymbol{k}T)^{1/2}\}^3 \cdot \exp(q/\boldsymbol{k}T). \quad (21)$$

The calculated values of $K_A^0 \equiv (1/\mathrm{k}T) \cdot h^3/(2\pi m\mathrm{k}T)^{3/2}$ are compared with the experimental value in Table 1. As can be seen in this table, K_A^0 (calc.) $\lesssim 5 \times 10^{-9}$ (atm^{-1}), while K_A^0 (expt.) $= 1 \times 10^{-3}$

TABLE 1
THE COMPARISON BETWEEN K_A^0 (calc.) AND K_A^0 (expl.) FOR THE IMMOBILE ADSORPTION[a]

Temperature, °C	K_A^0 (calc.), atm^{-1}	K_A^0 (expt.) atm^{-1}
400	5.2×10^{-9}	
500	3.7×10^{-9}	1×10^{-3}
600	2.7×10^{-9}	

[a] $K_A^0 = (1/\boldsymbol{k}T) \cdot h^3/(2\pi m\boldsymbol{k}T)^{3/2}$.

TABLE 2
THE COMPARISON BETWEEN K_A^0 (calc.) AND K_A^0 (expt.) FOR THE MOBILE ADSORPTION[a]

Temperature, °C	K_A^0 (calc.), atm^{-1}	K_A^0 (expt.), atm^{-1}
400	5.1×10^{-3}	
500	4.2×10^{-3}	1×10^{-3}
600	3.5×10^{-3}	

[a] $K_A^0 = 10^{-16} \cdot \sigma \cdot (1/\boldsymbol{k}T) \cdot h \cdot f_{vib}/(2\pi m\boldsymbol{k}T)^{1/2}$, σ = 600 Å^2, $f_{vib} = 10$ ($\tilde{\nu} = 70$ cm^{-1}).

(atm^{-1}). Namely, K_A (calc.) $\ll K_A$ (expt.) provided that q (calc.) = q (expt.). This result means that the immobile adsorption would not be taking place on the surface of liquid indium.

The adsorbed molecule may be regarded as mobile if the molecule is not constrained by an active center on the surface of liquid metal. The adsorbed molecule may have two-dimensional translational freedoms as well as a freedom of a vibrational motion perpendicular to the surface of liquid metal. The statistical thermodynamical expression of the adsorption coefficient for such mobile adsorption as described above is as follows (in atm^{-1}),

$$K_A = 10^{-16} \cdot \sigma \cdot (1/\boldsymbol{k}T) \cdot \{h/(2\pi m\boldsymbol{k}T)^{1/2}\} \times f_{vib} \cdot \exp(q/\boldsymbol{k}T), \quad (22)$$

where σ is the co-area of the adsorbed molecule and f_{vib} is a vibrational partition function corresponding to the vibrational motion of alcohol molecule perpendicular to the surface of liquid metal.

Kemball (*6*) obtained $\sigma = 30$ Å for *n*-butyl alcohol at 25°C from the adsorption data of this alcohol onto mercury. The co-area at 450°C is evaluated to be $\sim 6 \times 10^2$ Å^2, provided that the thermal expansion ($@_{ads}$) of the adsorbed alcohol is approximated by $@_{ads} = (@_{liq})^{2/3}$, where $@_{liq}$ is the thermal expansion of liquid alcohol and the value is $\sim 1 \times 10^{-3}$ °C^{-1}. The co-area of *sec*-BuOH would not be different much from the value of *n*-butyl alcohol.

The vibrational partition function f_{vib} is given by

$$f_{vib} = \{1 - \exp(-h\nu/\boldsymbol{k}T)\}^{-1}, \quad (23)$$

where ν is a frequency of the corresponding vibration. Kemball (*6*) estimated that the wave number $\tilde{\nu}$ of the vibrational motion of acetone adsorbed on mercury is 70 cm^{-1}. If the wave number of vibrational motion of *sec*-BuOH adsorbed on liquid indium is approximated by this value, i.e., 70 cm^{-1}, the vibrational partition function f_{vib} can be evaluated.

On the basis of the approximations described above, calculations of adsorption coefficient for the mobile adsorption were carried out. The calculated values of K_A^0 are compared with the experimental value in Table 2. It can be seen that the calculated values agree well with the experimental value. Therefore, the mobile adsorption is likely taking place in the primary stage of the dehydrogenation of *sec*-BuOH on the liquid indium catalyst.

The above-mentioned discussions give the following reaction scheme:

$$\textit{sec}\text{-BuOH (g)} + S \rightleftharpoons \textit{sec}\text{-BuOH* (mobile)}$$
$$\textit{sec}\text{-BuOH* (mobile)} \rightleftharpoons \text{Activated state}$$
$$\downarrow$$
$$H_2(g) + MEK(g) + S.$$

The energy diagram corresponding to this reaction scheme is given in Fig. 12. As can be seen in this figure, the true energy of activation is 41 kcal/mole. Theoretical analyses of this activation energy must provide realistic mechanism of activation of alcohol molecule adsorbed on the liquid indium. However, the analyses require quantum chemical treatments which have somewhat different character from the present work and were not included in this paper.

Applications of the absolute reaction-rate theory (*7*) to the present case throw some light on the problem of the activated state. If a localized immobile activated complex

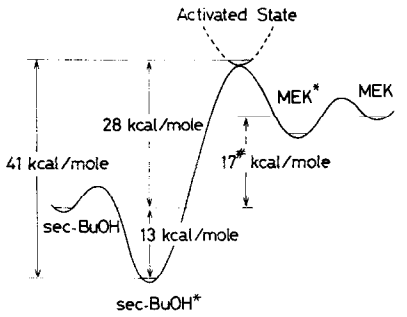

FIG. 12. The energy diagram for the dehydrogenation of *sec*-BuOH over the liquid indium catalyst (# represents an estimated value).

which is constrained by a two-dimensionally translating active center is considered, the theoretical rate constant is given by

$$k_1^0 = (\boldsymbol{kT}/h) \cdot h^3 \cdot F_a^* \cdot L \times \exp(-\epsilon/\boldsymbol{kT})/\{(2\pi m\boldsymbol{kT})^{3/2} \cdot b_g \cdot F_s\}, \quad (24)$$

where L is the number of active center per unit of surface area, F_a^* and F_s are the respective partition functions of the activated complex and the active center. Since $L \simeq 10^{15}/\text{cm}^2$ and $F_a^*/b_g F_s < 1$, the following inequality may result from Eq. (24),

$$k_1^0 < 10^{15} \times (\boldsymbol{kT}/h) \cdot h^3 \cdot \exp(-\epsilon/\boldsymbol{kT})/(2\pi m\boldsymbol{kT})^{3/2}. \quad (25)$$

According to the numerical calculations of this equation,* k_1^0 (calc.) $< 6.7 \exp(-\epsilon/\boldsymbol{kT})$ for *sec*-BuOH at 400°C. On the other hand, the experimental rate constant* was k_1^0 (expt.) $= 3 \times 10^6 \exp(-\epsilon/\boldsymbol{kT})$. Thus, it is clear that the assumption of the localized immobile activated complex is not adequate in the present case.

On the contrary, if a mobile activated complex is considered, the theoretical rate constant is given by

$$k_1^0 = (\boldsymbol{kT}/h) \cdot h \cdot b_a^* \cdot f_{vib}^* \times \exp(-\epsilon/\boldsymbol{kT})/\{(2\pi m\boldsymbol{kT})^{1/2} \cdot b_g\}, \quad (26)$$

where b_a^* is an internal partition function of the activated complex (a vibrational freedom along the reaction coordinate is not included) and f^*_{vib} is a partition function for the perpendicular vibrational freedom of the activated complex against the surface of the liquid metal. The two-dimensional motion of the activated complex on the surface was thought to be free from its localization due to a binding force of surface atom or atomic group of the liquid metal. Further, the activated complex for a unimolecular decomposition will have a loose molecular structure compared with that of the original molecule. Therefore, $b_a^* > b_g$ may be valid. In addition, inequality $f^*_{vib} > 10$ may be derived from the aforementioned discussions about f_{vib}, a partition function for the perpendicular vibrational freedom of adsorbed *sec*-BuOH against the surface of liquid indium. Thus, the following inequality results:

$$10^{-1} \times k_1^0 > (\boldsymbol{kT}/h) \cdot h \times \exp(-\epsilon/\boldsymbol{kT})/(2\pi m\boldsymbol{kT})^{1/2}. \quad (27)$$

A numerical calculation showed that k_1^0 (calc.) $> 1.1 \times 10^5 \cdot \exp(-\epsilon/\boldsymbol{kT})$ (cm/sec) for *sec*-BuOH at 400°C. This result is compared with the experimental rate constant k_1^0(expt.) $= 3 \times 10^6 \cdot \exp(-\epsilon/\boldsymbol{kT})$ (cm/sec). The comparison seems to show that the assumption of the mobile activated complex is adequate.

Possibilities in which other mechanisms have to be considered seem to be small. The diffusion rate-controlling mechanism was excluded by the fact that the reaction constant k_1 was independent of the diffusion coefficient D_{Ar}. Both the adsorption rate-controlling mechanism and the desorption rate-controlling mechanism were excluded because these mechanisms yield rate equations different from Eq. (7). Further, calculations based on a simple theory of gas–liquid solution equilibria proved that no significant amounts of alcohol vapor can dissolve into the liquid metal owing to the high surface tension of the liquid metal.

However, much yet remains to be clarified as to the details of the activation process. The proposed reaction scheme involves a somewhat mysterious state (activated state). Thus, the following steps seem to be worthy to be considered as the activation and the following reaction:

* Both k_1^0 (calc.) and k_1^0 (expt.) were expressed with the unit of [molecules/(cm² sec) (molecules/cm³)], i.e., [cm/sec].

$$sec\text{-}BuOH^* + M \longrightarrow sec\text{-}BuO^- M^+ + 1/2\ H_2\uparrow,$$
$$sec\text{-}BuO^- M^+ \xrightarrow{-H^-} MEK\uparrow + 1/2\ H_2\uparrow + M; \quad (A)$$

or alternatively,

$$sec\text{-}BuOH^* + 2M \rightleftarrows Et\text{—}\overset{\overset{OH}{|}}{\underset{\underset{Me}{|}}{C^+}}\ M^- + H^- M^+.$$
$$Et\text{—}\overset{\overset{OH}{|}}{\underset{\underset{Me}{|}}{C^+}}\ M^- + H^- M^+ \rightarrow MEK\uparrow + H_2\uparrow + 2M \quad (B)$$

where M indicates a metal atom.

The latter steps (B) are less likely, but not impossible at the reaction temperatures. The former steps (A) are reasonable considering from the ionization potential of indium.

Appendix

Outline of Solbrig-Gidaspow's Mathematical Treatment of the Rectangular Duct-Type Reactor.

The coordinating system for the analysis of the rectangular duct-type reactor is given

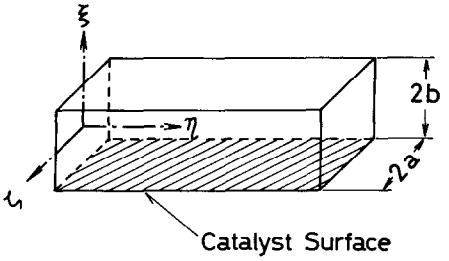

Fig. 13. The coordinate system for the rectangular duct with one catalytic wall.

in Fig. 13, and the nomenclature is given below:

$\gamma = a/b$, $z = \zeta/b$, $y = \xi/a$.
$D = 4a/(1+\gamma)$: Equivalent diameter of the duct.
D_{Ae}: Effective diffusion coefficient of reactant.
U: Mean linear flow-velocity of the fluid in the duct.
ρ_A: Mass concentration of the reactant.
ρ_{Ao}: Mass concentration of the reactant at the inlet of the reactor.
$C = \rho_A/\rho_{Ao}$
M_A: Molecular weight of the reactant.
N_R: Reynolds number defined by $UD\rho/\mu$ where μ is the viscosity of the fluid in the duct.
N_{Sc}: Schmidt number defined by $\mu/\rho D_{Ae}$.
n: Number of the reaction order.

From the material balance for the reactant with Fick's law of diffusion, the following steady mass balance equation for a small rectangular space $d\eta d\xi d\zeta$ in the reactor is derived.

$$V_\eta \frac{d\rho_A}{d\eta} = D_{Ae}\left(\frac{\partial^2\rho_A}{\partial\eta^2} + \frac{\partial^2\rho_A}{\partial\xi^2} + \frac{\partial^2\rho_A}{\partial\zeta^2}\right), \quad (1a)$$

where V_η expressing a laminar flow fluid velocity distribution is a complicated function (see original paper) of U, y, z, and the aspect ratio a/b.

When the diffusional term along the direction of the fluid flow can be neglected, Eq. (1a) becomes:

$$f(y,z)\frac{\partial C}{\partial xS} = \frac{\partial^2 C}{\partial y^2} + \gamma^2\frac{\partial^2 C}{\partial z^2}, \quad (2a)$$

where $f\ (y,z)$ is a function defined by

$$f(y,z) = V_\eta/(1.5\ U). \quad (3a)$$

The boundary conditions for the rectangular duct-type reactor with one catalytic wall are as follows;

$C(0, y, z) = 1$: at the inlet. (4a)
$\partial C/\partial y(x, 1, z) = 0$: at the upper wall. (5a)
$\partial C/\partial y(x, -1, z) = K_{wn}C^n$: at the lower wall (catalyst surface). (6a)
$\partial C/\partial z(x, y, \pm 1) = 0$: at the side wall. (7a)

K_{wn} is defined by

$$K_{wn} = (k_n a/D_{Ae})(\rho_{Ao}/M_A)^{n-1}. \quad (8a)$$

in which k_n is the rate constant of nth order reaction.

In order to solve the differential equation, Eq. (2a), with the boundary conditions of Eqs. (4a)–(7a), Solbrig and Gidaspow converted the differential equation into difference equation by employing such a finite-

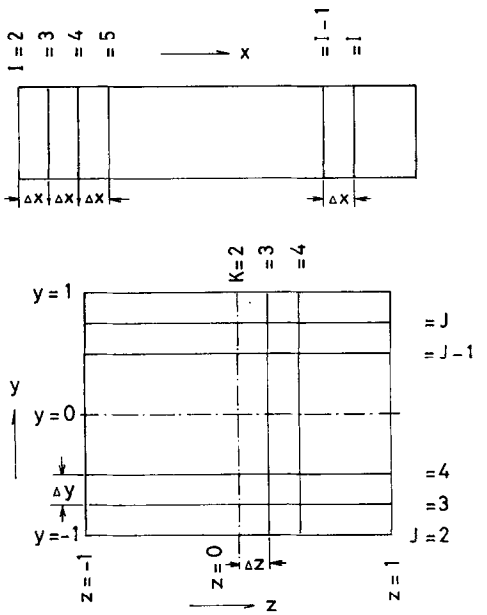

FIG. 14. Finite-difference grids employed for the mathematical analysis of the reaction in the rectangular duct type reactor.

difference grid model as shown in Fig. 14. The numerical solution of the difference equation gives a value for the reduced nondimensional concentration of the reactant C (x,y,z). Then, the mixing-cup concentration C_b of the reactant at a given dimensionless reduced distance x from the inlet is given by:

$$C_b = (3/8) \int_{-1}^{+1} \int_{-1}^{+1} C(x,y,z)\, f(y,z)\, dydz. \tag{9a}$$

This integration can be evaluated by using a two-dimensional analog of Simpson's rule.

Criteria for the Application of the Solbrig–Gidaspow's Treatment to the Present Reactor.

Laminar flow condition. The viscosity μ of the fluid in the reactor (mixed gas) was evaluated by the method of Hirschfelder (*8*) and the effective diffusion coefficient D_{Ae} of the reactant was evaluated by the method of Wilke (*9*). With these values of μ and D_{Ae}, Reynolds number N_R was evaluated to be less than 7.92 under the whole experimental conditions in the present work. Thus, the laminar flow condition $N_R < 2300$ was found to be satisfied.

Effect of foreflow region. The length of the foreflow region of the present reactor was estimated to be 0.08 cm by extending the treatment of Maeda *et al.* (*10*). The foreflow region is, therefore, less than 1% of the total length of the reactor (8.59 cm). No serious error due to the foreflow region can be considered in the calculated results.

Size of the finite-difference grid. The size of the finite-difference grid employed in this work is as follows:

$$y = 0.1,\ \Delta x/(\Delta y)^2 = \gamma^2 \Delta x/(\Delta z)^2 = 0.5.$$

Preliminary calculations showed that a smaller size grid than that described above gives little difference in the calculated results.

REFERENCES

1. SAITO, Y., MIYAMOTO, A., AND OGINO, Y., *Kogyo Kagaku Zasshi* **74**, 1521 (1971).
2. KASHIWADATE, K., SAITO, Y., MIYAMOTO, A., AND OGINO, Y., *Bull. Chem. Soc. Jap.* **44**, 3004 (1971).
3. OKANO, K., SAITO, Y., AND OGINO, Y., *Bull. Chem. Soc. Jap.* **45**, 69 (1972).
4. SAITO, Y., HIRAMATSU, N., KAWANAMI, N., AND OGINO, Y., *Bull. Jap. Petrol. Inst.* (in press).
5. SOLBRIG, C. W., AND GIDASPOW, D., *AICHE J.* **13**, 346 (1967).
6. KEMBALL, C., *Proc. Roy. Soc. Ser. A* **190**, 117 (1947).
7. GLASSTONE, S., LAIDLER, K. J., AND EYRING, H., "The theory of rate process." McGraw-Hill, New York, 1941.
8. HIRSCHFELDER, J. O., *J. Chem. Phys.* **16**, 968 (1948).
9. WILKE, C. R., *Chem. Eng. Progr.* **46**, 95 (1950).
10. SUGAWARA, T., TADAKI, T., AND MAEDA, S., *Kagaku Kogaku* **33**, 267 (1969).